Grafting of Poly(4-vinylpyridine) to Single-Walled Carbon Nanotubes and Assembly of Multilayer Films

Shuhui Qin,[†] Dongqi Qin,[†] Warren T. Ford,*[,†] Jose E. Herrera,[‡] and Daniel E. Resasco[‡]

Department of Chemistry, Oklahoma State University, Stillwater, Oklahoma 74078, and School of Chemical Engineering and Materials Science, University of Oklahoma, Norman, Oklahoma 73019

Received June 29, 2004; Revised Manuscript Received September 23, 2004

ABSTRACT: Poly(4-vinylpyridine) grafts to single-walled carbon nanotubes (SWNT) during in situ free radical polymerization of 4-vinylpyridine. After removal of catalyst particles and unattached polymer by centrifugation and ultrafiltration, the SWNT−PVP contains about 63 wt % SWNT by TGA. SWNT−PVP solutions in DMF, methanol, and 2-propanol are stable for at least 8 months. Atomic force microscopy images show individual tubes. Raman spectra are consistent with debundled SWNT having PVP covalently attached. Near-infrared (NIR) spectra show band gap electronic transitions of SWNT. Layer by layer deposition of alternating thin films of SWNT−PVP and poly(acrylic acid) (PAA) adds a constant amount of SWNT−PVP in each bilayer. FTIR spectra of the films show hydrogen bonding between the PVP and the PAA.

Introduction

Carbon nanotubes are under intensive investigation for nanostructures because they are metallic or semiconducting, exhibit ballistic transport, and have extremely high thermal conductivity and mechanical strength.[1] These properties will be exploited in many new polymer composites. Solution processing of polymer composites of single-walled carbon nanotubes (SWNT) requires dispersion of the inherently insoluble SWNT and the polymer into a solvent. One method to increase greatly the solubility of SWNT is chemical functionalization.[2−8] Numerous species have been added to the sidewalls of SWNT including fluorine,[9] aryl radicals,[10] aryl cations,[11] hydrogen,[12] nitrenes,[13,14] carbenes,[13,15] radicals, and 1,3-dipoles.[2,16,17] However, the electronic properties of SWNT are altered by heavy sidewall functionalization. Compared with small molecule adducts of SWNT, grafted polymers improve solubility with much less alteration of the electronic structure of SWNT because the long polymer chains provide many sites for solvation even with a low degree of functionalization.[18,19] Furthermore, covalent attachment of polymers helps to disperse SWNT into small bundles and individual tubes.

Previously we dispersed SWNT into water by in situ free radical polymerization of sodium 4-styrenesulfonate (NaSS) in the presence of SWNT to give aqueous solutions of SWNT that are stable for at least 1 year.[19] The proposed mechanism for the process is as follows. (1) The propagating poly(4-styrenesulfonate) (PSS) macroradicals add to the outermost layer of the bundles of SWNT. (2) Strong van der Waals attraction of the PSS to the SWNT overcomes the intertube van der Waals attractions and breaks the bundles apart. (3) The ionic functional groups of the PSS enable the SWNT−PSS to dissolve in water. Removal of catalyst residues and amorphous carbon by centrifugation and removal of unattached PSS by either ultrafiltration or ultracentrifugation give a stable aqueous solution with a 55/45 weight ratio of SWNT/PSS. Multiwall carbon nanotubes (MWNT) were functionalized also with polystyrene using similar procedure.[20]

Now we report the grafting of poly(4-vinylpyridine) (PVP) to SWNT by in situ free radical polymerization in DMF. The process requires no pretreatment of SWNT and works well with as-received HiPco SWNT. Debundling and functionalization of SWNT are achieved in one step. The dispersion of SWNT−PVP contains individual tubes and forms alternating multilayer thin films with poly(acrylic acid) (PAA).

Experimental Section

Materials. SWNT (BuckyPearls, HiPco batch P0205) were used as received from Carbon Nanotechnologies Inc., Houston, TX. 4-Vinylpyridine (Aldrich, 95%) was vacuum-distilled twice before use. Azobis(isobutyronitrile) (AIBN) was crystallized from methanol. PAA (M_w = 100 000) and branched poly(ethylenimine) (PEI) (M_w = 70 000) were used as received from Aldrich. All other reagents and solvents were used as received from Aldrich or Acros Chemicals. Water was triply deionized with a Barnstead E-pure system to conductivity less than 1×10^{-6} ohm^{-1} cm^{-1}.

Instruments and Measurements. The separations of SWNT−PVP from the impurities were performed with a IEC centrifuge Size 2, Model EXD instrument at 6000*g* and by ultrafiltration through a 0.2 μm PTFE membrane. Water bath sonication was performed with a FS30 (Fisher Scientific) sonicator. Thermogravimetric analyses were performed with a Shimadzu TGA50/50H instrument. Raman spectra were recorded on a Jovin Yvon-Horiba Lab Raman spectrometer equipped with a CCD detector and 514 nm laser excitation. Near-IR spectra were recorded on Bruker Equinox 55 FTIR/FTNIR instrument. The samples for Raman and near-IR measurements were dip-coated from a dilute DMF solution of SWNT−PVP onto a glass coverslip and air-dried. Atomic force micrographs were obtained using a Multimode Nanoscope IIIa SPM (Digital Instruments, St. Barbara, CA) operating in the tapping mode under ambient conditions using Si cantilevers with a spring constant of about 20 N/m and a resonance frequency of about 265 kHz. The set-point amplitude ratio was maintained at 0.9 to minimize sample deformation by the tip. The samples for AFM measurements were dip-coated from dilute solutions in DMF onto a freshly cleaved mica surface

[†] Oklahoma State University.
[‡] University of Oklahoma.
* Corresponding author. E-mail wtford@okstate.edu.

10.1021/ma048692p CCC: $27.50
Published on Web 11/24/2004

and air-dried. Mid-IR spectra of a film of five bilayers of (SWNT−PVP/PAA) on a CaF_2 plate were recorded on a Perkin-Elmer 2000 FTIR instrument. Transmission UV−vis spectra were recorded from thin films coated on quartz on a Hewlett-Packard 8453A diode array spectrophotometer. ^{1}H NMR spectra were recorded at 300 MHz on a Varian Gemini spectrometer.

Polymerization and Purification. A 50 mL dried Schlenk flask was charged with a magnetic stirrer, 25 mg of SWNT, and 35 mL of DMF. After stirring for 6 h at room temperature, 40 mg of AIBN and 5.0 g of 4-VP were added, and the mixture was degassed by four freeze−pump−thaw cycles. The flask was placed in a thermostated oil bath at 65 °C under stirring. After 48 h the mixture was cooled to room temperature, diluted to 300 mL with fresh DMF, bath sonicated for 1 h, and centrifuged for 6 h. After removal of the homogeneous black supernatant, the black sediment (mainly carbon-coated iron particles and unreacted large SWNT bundles) was redispersed in DMF by stirring and centrifuged for 3 h, and the supernatant was collected. The centrifugation procedure was repeated two times.

The combined black solution was vacuum-filtered through a 0.2 μm PTFE membrane and washed 10 times with 40 mL of DMF for each time. All of the solid was dissolved in 100 mL of DMF, and 30 mL of the solution was dried to obtain 8.1 mg of solid. The ^{1}H NMR spectrum of SWNT−PVP showed broad signals at 1.0−2.5, 6.2−7.2, and 7.7−8.7 ppm. The ^{1}H NMR spectrum of PVP from the ultrafiltrate showed narrower signals from PVP and signals from a trace of monomeric 4-vinylpyridine.

In a control experiment, 5 mg of pristine SWNT, 1.0 g of PVP (recovered from the filtrate of the grafted SWNT−PVP), and 7 mL of DMF were stirred for 48 h at 65 °C, diluted to 60 mL with DMF, and sonicated for 1 h. The SWNT precipitated, leaving a slightly gray DMF solution.

(SWNT−PVP/PAA)$_n$ Multilayer Films. A 1.0 × 0.5 cm^2 quartz wafer was cleaned with 30% H_2O_2 and concentrated sulfuric acid (3:7 in volume) at 100 °C for 30 min and rinsed 10 times with water. The wafer was immersed in an aqueous PEI solution (1 mg/mL) for 10 min, rinsed by dipping three times into water for 1 min, immersed in solution of PAA in methanol (1.0 mg/mL) for 5 min, and rinsed by dipping three times into methanol for 1 min. Bilayers of (SWNT−PVP/PAA) were coated by alternately dipping into a methanol solution of SWNT−PVP (0.5 mg/mL) for 20 min, rinsing with methanol three times, dipping into the PAA solution for 5 min, and rinsing three times with methanol. PVP/PAA multilayer films were fabricated from methanol solutions of PVP (1.0 mg/mL) and PAA (1.0 mg/mL) by the same procedure.

Results and Discussion

The grafting of PVP to SWNT was carried out by dispersing the SWNT in a DMF solution of 4-vinylpyridine and polymerizing with AIBN as a radical initiator as shown in Scheme 1. The procedure was similar to that used for grafting of PSS to SWNT in water.[19] DMF is a good solvent for the dispersion of SWNT.[21,22] Residual catalyst and excess unbound PVP were removed by gentle centrifugation and ultrafiltration. The mat of SWNT−PVP that was collected by ultrafiltration was dissolved by stirring or water bath sonication in DMF, methanol, and 2-propanol to give 0.27 mg mL^{-1} solutions that were stable for at least 8 months. In a control experiment, stirring for 48 h at 65 °C with PVP in DMF failed to disperse the pristine SWNT, which indicates that the stable SWNT solution is not due to adsorption of PVP.

TGA of the SWNT−PVP gave 39% weight loss in a nitrogen atmosphere at 600 °C (Figure 1a-1), indicating that the composite contained 39% PVP. In a control experiment all of the bulk PVP was lost at <450 °C in nitrogen as shown in Figure 1a-3. To test for possible

Scheme 1

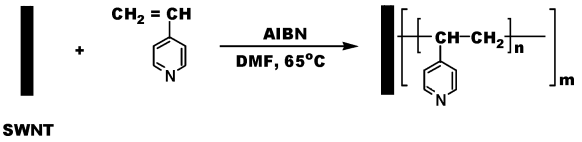

formation of stable carbonaceous product from PVP and SWNT during the pyrolysis of SWNT−PVP, a 30/70 weight ratio of pristine SWNT and the PVP that was recovered from the ultrafiltrate of the grafted SWNT−PVP was ground with a mortar and pestle. The weight loss during TGA of the ground mixture matched well with the theoretical value as shown in Figure 1a-2, which supports the conclusion that the entire PVP component in SWNT/PVP was lost during TGA. By TGA in air, both SWNT and PVP were lost from the composite at 600 °C to leave less than 1 wt % of catalyst residue (Figure 1b-1,3). About 18% of iron oxide (presumed to be Fe_2O_3) was left from the pristine SWNT (Figure 1b-2), which is consistent with the metal impurity (Fe, 13%) in pristine SWNT provided by the manufacturer. Therefore, the composite contains SWNT and PVP, with a 61/39 weight ratio and <1 wt % of catalyst. Moreover, the procedure recovered 68% of the original carbon material in the form of both individual and bundles of SWNT−PVP. Purifications of HiPco SWNT by dispersal with a variety of surfactants and polymers by high shear mixing, sonication, and ultracentrifugation recovered from the supernatant less than 10% of the original carbon that was highly enriched in individual SWNT.[23] The much larger amounts recovered after polymer grafting are due to redispersion of the mat of solid carbon material from ultrafiltration with the supernatant.

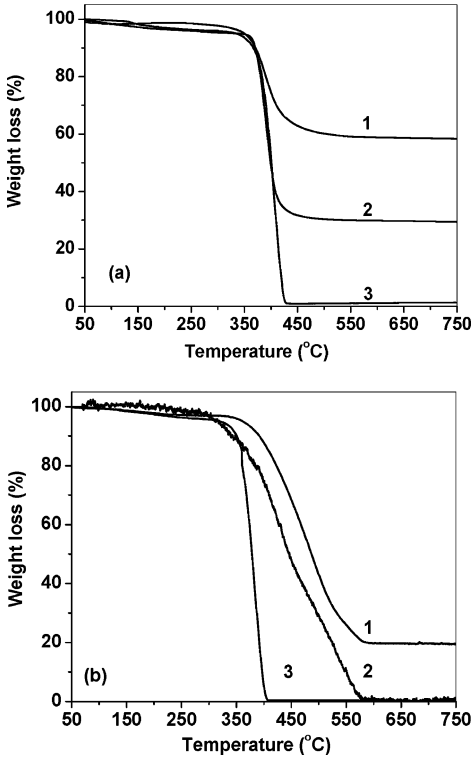

Figure 1. (a) TGA thermograms of SWNT−PVP (1), a mixture of SWNT and PVP in a 30/70 weight ratio (2), and PVP (3) in a nitrogen atmosphere. (b) TGA thermograms of pristine SWNT (1), SWNT−PVP (2), and PVP (3) in air.

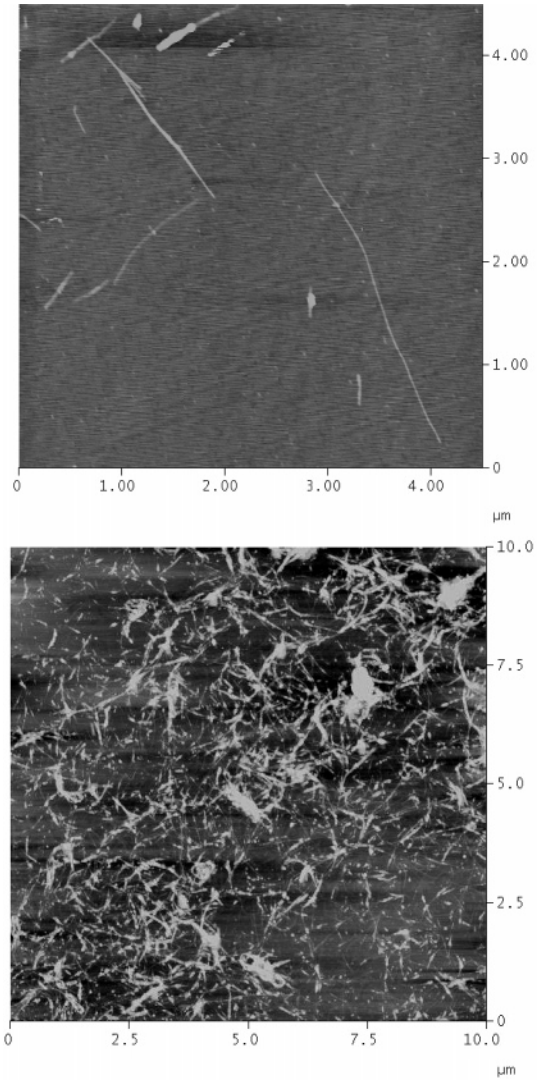

Figure 2. AFM height images of SWNT−PVP on a mica surface.

The distribution of diameters and lengths of the functionalized SWNT were determined by tapping mode AFM. The images in Figure 2 show individual SWNT and bundles of tubes. The contour lengths range from several hundred nanometers to several micrometers. The heights of tubes range from 0.8 to 3.2 nm with an average of 1.5 nm from 30 measurements of different tubes and of the same tube at different positions. The diameters of individual pristine HiPco SWNT range from 0.6 to 1.3 nm.[24] Since the PVP chains thicken the contour of SWNT in AFM images, the 1.5 nm height of the SWNT−PVP is consistent with single tubes. Some long single tubes had different heights at different locations on the tube, indicating that not all of the tube surfaces were covered by PVP or that what appeared to be one tube was actually overlapping tubes.

Figure 3 shows the Raman spectra of both pristine SWNT and SWNT−PVP composite from 514 nm laser excitation. The spectrum of pristine SWNT has peaks from the radial breathing modes (RBM) at 150−320 cm^{-1}, the G-band at 1500−1600 cm^{-1}, and a very weak disorder peak (the D-band) at 1300−1400 cm^{-1}, which is attributed to scattering from sp^3 carbon defects in the side walls of the SWNT. An inverse relation between the RBM peak frequencies and the diameters of the nanotubes is well established.[25,26] Although the resonance Raman spectrum from excitation at a single wavelength does not detect all types of tubes in the sample, and 514 nm excitation detects mainly metallic SWNT, several peaks in the RBM region indicate a distribution of nanotube diameters. The SWNT−PVP shows basically the same Raman spectral pattern as pristine SWNT. Compared with the spectrum of pristine SWNT, the D-band in SWNT−PVP is enhanced. Since the adsorption of surfactants and polymers has little effect on the D-band, the Raman results support covalent functionalization of the nanotube sidewalls. In the RBM region of the spectrum of SWNT−PVP (Figure 3 inset), the peaks are shifted to higher frequency by 5−8 cm^{-1} relative to those of pristine SWNT, indicating that the grafting of PVP had little effect on the distribution of diameters of the SWNT detected. An upshift of about 3 cm^{-1} also occurred in the G-band. The peak ratios in the G-band also changed. This upshift has been attributed to debundling.[27,28]

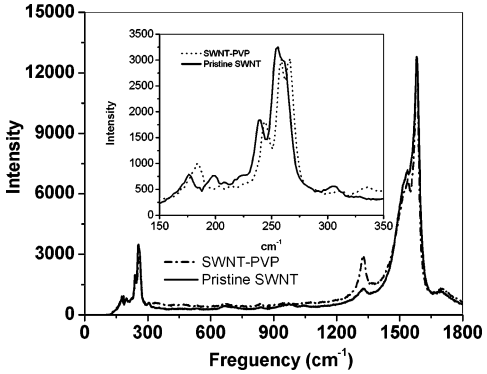

Figure 3. Raman spectra of solid SWNT−PVP and pristine SWNT from 514 nm laser excitation.

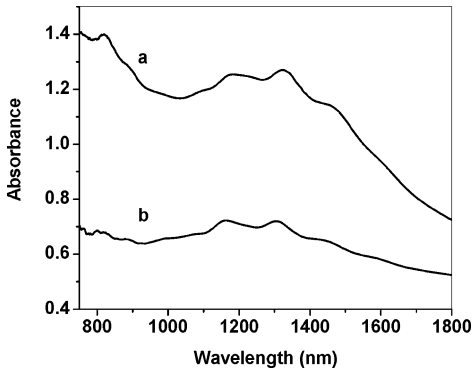

Figure 4. Transmission near-infrared spectra of films of pristine SWNT (a) and SWNT−PVP (b).

Chemical functionalization of the nanotube surface alters the electronic structure. The low-energy, interband, electronic transitions of SWNT appear in the near-infrared spectrum. In Figure 4, the near-IR spectrum of SWNT−PVP still shows the interband transitions, but with an average shift to lower wavelength by 21 nm due to alteration of the π-electron system. Therefore, the near-IR spectrum supports a low density of PVP chains added to the SWNT side walls, which agrees with the Raman and TGA results. Heavy functionalization of SWNT leaves no discernible peaks in the near-IR spectrum.[10,11]

Layer by Layer Thin Films. Incorporation of SWNT should enhance the electrical conductivity and the mechanical strength of thin polymer films. Multilayer films of SWNT−PVP/PAA and PVP/PAA were fabri-

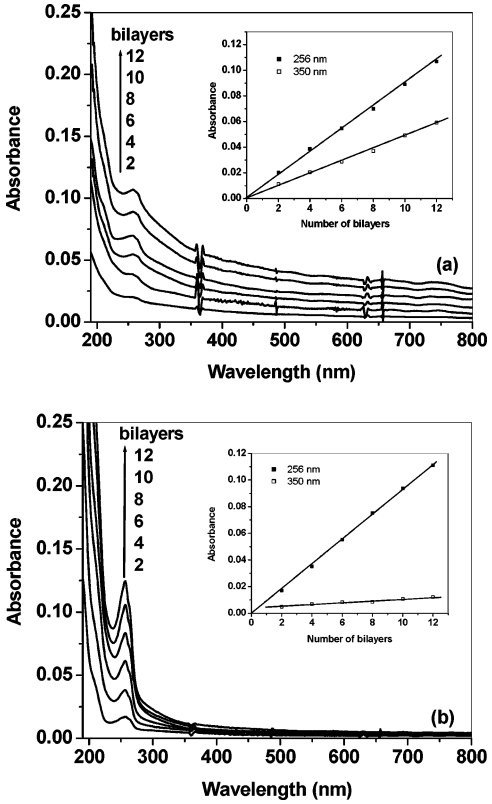

Figure 5. Transmission UV−vis absorption spectra of SWNT−PVP/PAA (a) and PVP/PAA (b) multilayer films with different numbers of bilayers.

cated using methanol solutions for LBL deposition on a quartz substrate.[29] Robust LBL films of PVP and PAA have been fabricated before based on hydrogen bonding between pyridine and carboxylic acid groups.[30] The thickness of the bilayers can be adjusted by changing the concentrations and the molecular weights of both polymers. Figure 5a shows the UV−vis absorption spectra of the SWNT−PVP multilayer film with different numbers of bilayers. Using absorption at 256 nm to measure PVP and absorption at 350 nm to measure SWNT, the linear increases of absorbance with number of bilayers deposited indicate uniform thicknesses of the bilayers of both SWNT−PVP/PAA and PVP/PAA (insets of Figure 5a,b). The absorbance of PVP at 256 nm in the SWNT−PVP/PAA films is slightly weaker than that in the PVP/PAA films having the same number of bilayers because the concentration of SWNT−PVP (0.5 mg/mL) used for depositions was lower than that of PVP (1.0 mg/mL).

The AFM image in Figure 6 of a SWNT−PVP/PAA multilayer film on a silicon wafer shows SWNT several hundred nanometers to several micrometers in length and a relatively smooth polymer surface. The SWNT on the surface of a film having PAA as the last layer deposited indicate mixing of the PVP and PAA in the film.

The driving force for the LBL film fabrication was identified by mid-IR spectroscopy. Figure 7a shows the spectra of pure PVP, SWNT−PVP, and PAA on CaF_2 plates. The spectra of PVP and SWNT−PVP are basically the same due to strong absorption by PVP and weak absorption of SWNT. The broad peak at 1708 cm^{-1} in the spectrum of PAA alone (Figure 7a) is due to hydrogen-bonded carboxylic acid groups. Figure 7b shows the IR spectra of five bilayer $(SWNT−PVP/PAA)_5$

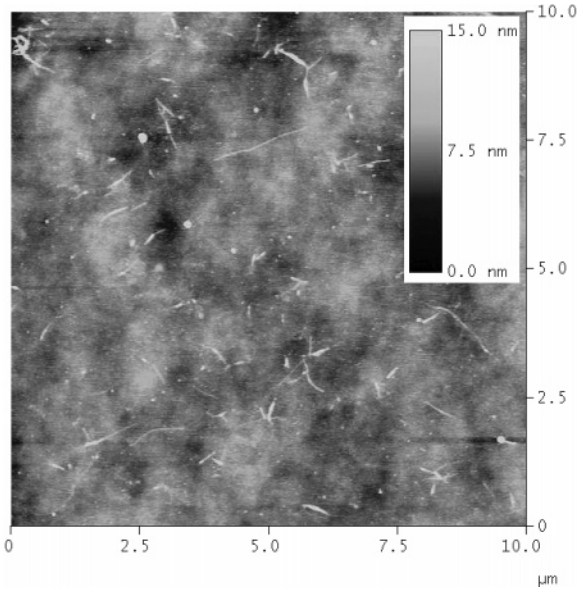

Figure 6. AFM height image of a $(SWNT−PVP/PAA)_5$ multilayer film.

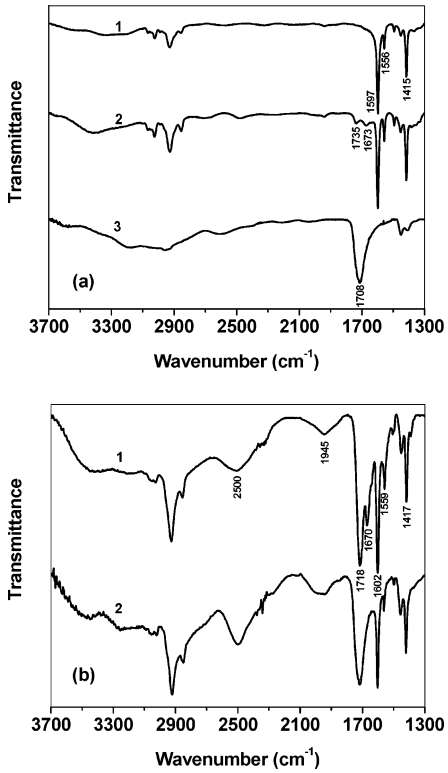

Figure 7. Transmission FTIR spectra of (a) cast films of pure PVP (1), SWNT−PVP (2), pure PAA (3) and (b) $(SWNT−PVP/PAA)_5$ (1) and $(PVP/PAA)_5$ (2) multilayer films on a CaF_2 plate.

and $(PVP/PAA)_5$ films. The carbonyl stretching vibration of the SWNT−PVP/PAA film at 1718 cm^{-1} shows that the carboxylic acid groups are in a less associated state than in PAA alone. The bands due to pyridine groups in SWNT−PVP shifted from 1415, 1556, and 1597 cm^{-1} to 1417, 1559, and 1602 cm^{-1} after assembly with PAA, indicating interaction between PAA and PVP.[30,31] Furthermore, the O−H stretching vibrations at 2500 and 1945 cm^{-1} indicate a strong hydrogen bonding between the carboxylic acid of PAA and the pyridine groups of PVP.[30−32] Thus, hydrogen bonding is the driving force for the SWNT−PVP/PAA film construction. The PVP/

PAA film has basically the same IR spectrum as the SWNT−PVP/PAA film. Thus, the PVP adheres strongly to PAA in the films by hydrogen bonding both in the presence and in the absence of SWNT.

In conclusion, chemical functionalization by in situ polymerization of 4-vinylpyridine is an effective method for solubilization of HiPco SWNT and for removal of catalyst impurities. Raman and near-IR spectra, and the 61/39 SWNT/PVP composition of the material, support grafting of the polymer to the sidewalls of the SWNT. The SWNT−PVP dissolves well in good solvents for PVP. Alternating layers of SWNT−PVP and PAA in LBL films adhere strongly by hydrogen bonding. Thicker films will be prepared to determine the effect of SWNT on the electrical conductivity and the mechanical strength.

Acknowledgment. Financial support from the National Science Foundation (EPS-0132543) is gratefully acknowledged. We thank LeGrande Slaughter for use of the TGA.

References and Notes

(1) Dresselhaus, M. S.; Dresselhaus, G.; Avouris, P. *Carbon Nanotubes: Synthesis, Structure, Properties and Applications*; Springer-Verlag Press: Heidelberg, 2001.
(2) Hirsch, A. *Angew. Chem., Int. Ed.* **2002**, *41*, 1853−1859.
(3) Bahr, J. L.; Tour, J. M. *J. Mater. Chem.* **2002**, *12*, 1952−1958.
(4) Lin, T.; Bajpai, V.; Ji, T.; Dai, L. M. *Aust. J. Chem.* **2003**, *56*, 635−651.
(5) Qin, S. H.; Oin, D. Q.; Ford, W. T.; Resasco, D. E.; Herrera, J. E. *J. Am. Chem. Soc.* **2004**, *126*, 170−176.
(6) Qin, S. H.; Qin, D. Q.; Ford, W. T.; Resasco, D. E.; Herrera, J. E. *Macromolecules* **2004**, *37*, 752−757.
(7) Kong, H.; Gao, C.; Yan, D. Y. *J. Am. Chem. Soc.* **2004**, *126*, 412−413.
(8) Yao, Z. L.; Braidy, N.; Botton, G. A.; Alex, A. T. *J. Am. Chem. Soc.* **2003**, *125*, 16015−16024.
(9) Mickelson, E. T.; Huffman, C. B.; Rinzler, A. G.; Smalley, R. E.; Hauge, R. H.; Margrave, J. L. *Chem. Phys. Lett.* **1998**, *296*, 188−194.
(10) Bahr, J. L.; Yang, J. P.; Kosynkin, D. V.; Bronikowski, M. J.; Smalley, R. E.; Tour, J. M. *J. Am. Chem. Soc.* **2001**, *123*, 6536−6542.
(11) Dyke, C. A.; Tour, J. M. *J. Am. Chem. Soc.* **2003**, *125*, 1156−1157.
(12) Pekker, S.; Salvetat, J. P.; Jakab, E.; Bonard, J. M.; Forro, L. *J. Phys. Chem. B* **2001**, *105*, 7938−7943.
(13) Holzinger, M.; Vostrowsky, O.; Hirsch, A.; Hennrich, F.; Kappes, M.; Weiss, R.; Jellen, F. *Angew. Chem., Int. Ed.* **2001**, *40*, 4002−4005.
(14) Holzinger, M.; Abraham, J.; Whelan, P.; Graupner, R.; Ley, L.; Hennrich, F.; Kappes, M.; Hirsch, A. *J. Am. Chem. Soc.* **2003**, *125*, 8566−8580.
(15) Chen, Y.; Haddon, R. C.; Fang, S.; Rao, A. M.; Lee, W. H.; Dickey, E. C.; Grulke, E. A.; Pendergrass, J. C.; Chavan, A.; Haley, B. E.; Smalley, R. E. *J. Mater. Res.* **1998**, *13*, 2423−2431.
(16) Ying, Y. M.; Saini, R. K.; Liang, F.; Sadana, A. K.; Billups, W. E. *Org. Lett.* **2003**, *5*, 1471−1473.
(17) Georgakilas, V.; Kordatos, K.; Prato, M.; Guldi, D. M.; Holzinger, M.; Hirsch, A. *J. Am. Chem. Soc.* **2002**, *124*, 760−761.
(18) Viswanathan, G.; Chakrapani, N.; Yang, H. C.; Wei, B. Q.; Chung, H. S.; Cho, K. W.; Ryu, C. Y.; Ajayan, P. M. *J. Am. Chem. Soc.* **2003**, *125*, 9258−9259.
(19) Qin, S. H.; Qin, D. Q.; Ford, W. T. *Macromolecules* **2004**, *37*, 3965−3967.
(20) Shaffer, M. S. P.; Koziol, K. *Chem. Commun.* **2002**, 2074−2075.
(21) Ausman, K. D.; Piner, R.; Lourie, O.; Ruoff, R. S.; Korobov, M. *J. Phys. Chem. B* **2000**, *104*, 8911−8915.
(22) Krupke, R.; Hennrich, F.; Hampe, O.; Kappes, M. M. *J. Phys. Chem. B* **2003**, *107*, 5667−5669.
(23) Moore, V. C.; Strano, M. S.; Haroz, E. H.; Hauge, R. H.; Smalley, R. E.; Schmidt, J.; Talmon, Y. *Nano Lett.* **2003**, *3*, 1379−1382.
(24) Bachilo, S. M.; Strano, M. S.; Kittrell, C.; Hauge, R. H.; Smalley, R. E.; Weisman, R. B. *Science* **2002**, *298*, 2361−2366.
(25) Dresselhaus, M. S.; Dresselhaus, G.; Jorio, A.; Souza, A. G.; Saito, R. *Carbon* **2002**, *40*, 2043−2061.
(26) Doorn, S. K.; Heller, D. A.; Barone, P. W.; Usrey, M. L.; Strano, M. S. *Appl. Phys. A: Mater. Sci. Process.* **2004**, *78*, 1147−1155.
(27) Stephan, C.; Nguyen, T. P.; de la Chapelle, M. L.; Lefrant, S.; Journet, C.; Bernier, P. *Synth. Met.* **2000**, *108*, 139−149.
(28) Rao, A. M.; Chen, J.; Richter, E.; Schlecht, U.; Eklund, P. C.; Haddon, R. C.; Venkateswaran, U. D.; Kwon, Y. K.; Tomanek, D. *Phys. Rev. Lett.* **2001**, *86*, 3895−3898.
(29) Decher, G. *Science* **1997**, *277*, 1232−1237.
(30) Wang, L. Y.; Fu, Y.; Wang, Z. Q.; Fan, Y. G.; Zhang, X. *Langmuir* **1999**, *15*, 1360−1363.
(31) Fu, Y.; Bai, S. L.; Cui, S. X.; Qiu, D. L.; Wang, Z. Q.; Zhang, X. *Macromolecules* **2002**, *35*, 9451−9458.
(32) Kumar, U.; Kato, T.; Frechet, J. M. J. *J. Am. Chem. Soc.* **1992**, *114*, 6630−6639.

MA048692P